Phys. Status Solidi A **212,** No. 10, 2309–2314 (2015) / **DOI** 10.1002/pssa.201532136

physica status solidi a
www.pss-a.com
applications and materials science

Synthesis and double-hierarchical structure of MoS_2/C nanospheres

Lyudmyla Shyyko*[,1], Volodymyr Kotsyubynsky[,1], Ivan Budzulyak[1], Michal Rawski[2], Yurij Kulyk[3], and Roman Lisovski[4]**

[1] Department of Materials Science and New Technology, Vasyl Stefanyk Precarpathian National University, Shevchenko Street 57, 76018 Ivano-Frankivsk, Ukraine
[2] Analytical Laboratory of the Faculty of Chemistry, Maria Curie-Sklodowska University, M. Curie-Sklodowska Square 3, 20031 Lublin, Poland
[3] Department of Physics of Metals, Ivan Franko Lviv National University, Kyrylo and Mefodiy Street 8, 79005 Lviv, Ukraine
[4] G.V. Kurdyumov Institute for Metal Physics of the N.A.S. of Ukraine, 36 Acad. Vernadsky Boulevard, 03680 Kyiv, Ukraine

Received 3 March 2015, revised 17 June 2015, accepted 26 June 2015
Published online 17 July 2015

Keywords carbon, $C_{19}H_{42}BrN$, double-hierarchical structures, hydrothermal synthesis, MoS_2, nanoparticles

* Corresponding author: e-mail liudmyla.shyiko@pu.if.ua, Phone: +380673436942
** e-mail kotsuybynsky@gmail.com, Phone: +380973803959

The results of MoS_2/carbon nanocomposite hydrothermal synthesis is presented. The synthesized material was studied by XRD, TEM, EDS, SAXS, and porosimetry. The multilayer nanospheres with the average size 40–70 nm were obtained. The investigations confirm the formation of particles with double-hierarchical structure where 2H-MoS_2 layers alternate with carbon layers. Atomic ratio of MoS_2:C is about 1:1 (at.%) and does not depend on the heat treatment.

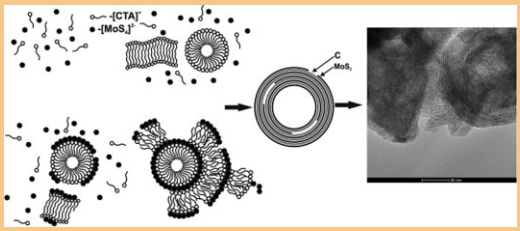

The proposed formation mechanism of MoS_2/C double-hierarchical structure.

1 Introduction The peculiarities of layered metal chalcogenides MX_2 ($M = W$, Mo; $X = S$, Se) crystal and electronic structures cause physical properties that cannot be equivalently replicated in other materials. Applications of such materials are expanded in case of nanostructured systems with specified morphological characteristics. As example of this approach realization can be solid radiation-resistive antifriction materials adapted for use in a wide temperature range and nanocrystal additives for industrial oils, hydrogen sensors, highly anisotropic semiconductive nanomaterials for electrochemical devises, catalysts, insulation nanomaterials with ultra low values of thermal conductivity. Much attention is paid to the obtaining of fullerene-like structures based on layered metal chalcogenides [1], which are expected to be used as lubricants [2] or as components of nanocomposite structures [3, 4]. Another promising application of such systems is electrode for lithium-ion power sources [5–8]. In this case the main point is the experimental method, which allows to obtain a material with specifically modified structural and morphological characteristics. One of the controlling leverages is the use of different additives, such as surfactants and templates. For instance, using surfactant and varying its type and concentration it became possible to preset size and shape of desirable particles, in such way atomically thin nanosheets [9], nanoflowers [10, 11], nanotubes, nanoribbons [12], hexagonal, or platelet-like particles [13] were obtained. In addition, surfactants can modify the phase interfaces sufficiently to get the optimal conditions for the fabrication of useful composites based on normally incompatible materials [26]. In such way, with assistance of different cationic surfactants (CTAB, DTAB, OTAB, and TBAB) the heterolayered molybdenum disulfide/graphene composites were synthesized, which exhibited remarkable electrochemical

performances including highly reversible specific capacity, excellent cycling performance, and enhanced high-rate capability [14]. In this case, graphene in form of the highly ordered carbon sheets resolve a shortcoming as low-electric conductivity.

This article considers the experimental aspects of the obtaining the ultrafine nanostructured material which unites molybdenum disulfide and carbon with fullerene-like morphology of the particles by hydrothermal synthesis using cetyltrimethylammonium bromide as a micelle forming agent.

2 Materials and methods

2.1 Materials preparation The synthesis of double-hierarchical structure of MoS_2/C was carried out in two steps. In the first stage 9.8 g of $(NH_4)_2MoO_4$ was dissolved in 68 ml of 20% $(NH_4)_2S$. After stirring for 30 min at room temperature the dark yellow precipitate of $(NH_4)_2MoS_4$ was formed (Eq. (1)):

$$(NH_4)_2MoO_4 + 4(NH_4)_2S \rightarrow (NH_4)_2MoS_4 + 8NH_4 \cdot OH. \quad (1)$$

In the second stage, the resulting $(NH_4)_2MoS_4$ was mixed with 3.3 ml of hydrazine hydrate $N_2H_4 \cdot N_2O$ and 100 ml of distilled water. The pH level of the reaction medium was 7.8 and regulated by hydrochloric acid HCl. After adding 3 g of cetyltrimethylammonium bromide $C_{19}H_{42}BrN$, the solution was put into Teflon autoclave and stored at the temperature of 220 °C for 24 h. The resulting black precipitate was washed with distilled water and ethanol, and after centrifugation, dried at 80 °C. Additionally, the obtained material was annealed in argon atmosphere at 500 and 1000 °C for 2 h. The experiment is based on the approaches of MoS_2 nanostructures synthesis, in particular [15].

2.2 Materials characterization The synthesized material phase composition and structure were investigated by XRD and SAXS (DRON-3 diffractometer, CuK_α radiation). Morphological characteristics and chemical composition were obtained by TEM and EDS (FEI Technai G2 X-TWIN Microscope). The specific surface area and pore size distribution were measured by nitrogen adsorption at 77.2 K (Quantachrome NOVA 2200e Porosimeter).

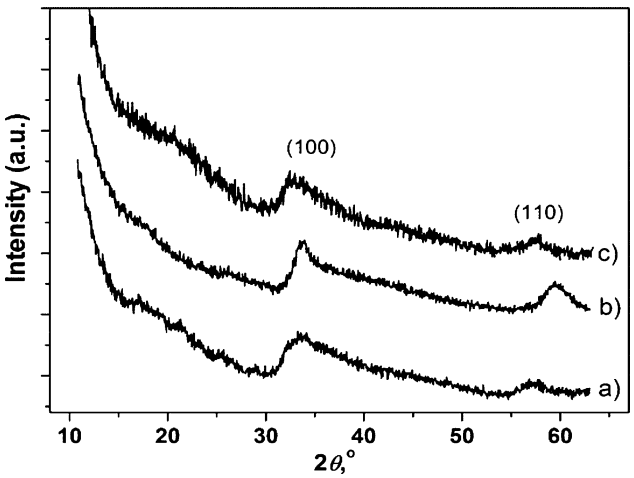

Figure 1 Diffraction patterns of obtained materials after heat treatment at 80 °C (a), 500 °C (b), and 1000 °C (c).

3 Results According to the results of X-ray diffraction the resulting material is in a state close to the X-ray amorphous. In the diffraction, pattern of the material obtained in situ and dried at 80 °C (Fig. 1, curve a) there can be seen two areas of intensity growth of diffracted rays: in the 2θ angle ranges of 30–38° and 56–59°, which can be associated with (100) and (110) reflections that characterize the 2H-MoS_2 crystal structure (Fig. 2a), which belongs to the hexagonal system, symmetry space group P63/mmc, typical values of lattice constants are $a = 0.3161$ nm, $c = 1.2295$ nm [16]. Maximum intensity of the (002) reflection in the vicinity of $2\theta = 14$–15^o is not observed, that is analogous to the results of several works [16, 6–8]. In this case, the transition of 2H-MoS_2 into nano-dispersed state was accompanied by a significant decline in the intensity of the (002) and (103) reflections while the intensities of the (100) and (110) reflections increase.

In accordance with Refs. [17, 14], the lack of the (002) reflection indicates the absence of connection between individual layers of MoS_2, and the formation of the graphene-like material. The obtained diffraction patterns are very similar to the data of Ref. [15] for the case of nanodispersed MoS_2, synthesized by hydrothermal method without surfactant in the reaction medium.

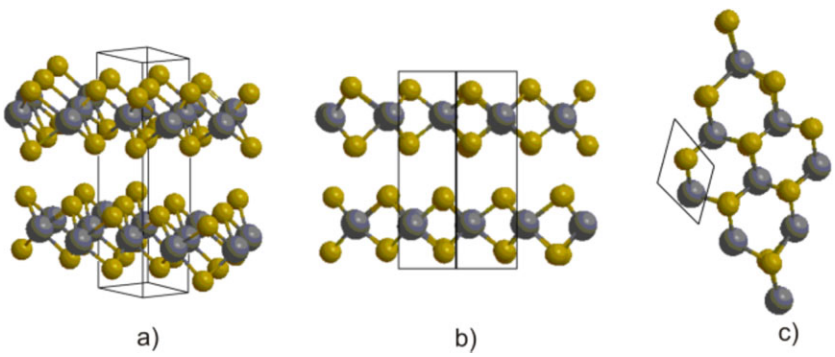

Figure 2 The crystal structure of 2H-MoS_2, where gray balls are Mo atoms and yellow are S atoms (a), view along the [110] (b), and [001] direction (c), the unit cell is additionally selected.

Annealing in the inert atmosphere of argon at 500 °C for 2 h resulted in a reduction of the width of the (100) and (110) reflections, but the condition of the material remained close to the X-ray amorphous (Fig. 1, curve b). The peculiarity of this diffraction is the displacement of the reflection, which corresponds to the family of (110) planes on 2.2°, while the position of the (100) reflection did not change within the error. Position of the (110) reflection on diffraction pattern for the annealed material is close to the values typical for microcrystalline samples of 2H-MoS_2. Thereby in the material there is a change of the interatomic distances in the (001) plane, i.e., along the layers formed by Mo atoms placed between two layers of S atoms, which form a trigonal prism (Fig. 2b and c).

On the diffraction pattern of the material obtained by the sample annealing in the stream of argon at 1000 °C any significant changes were not observed, this fact confirmed the temperature stability of the material (Fig. 1, curve c).

According to the TEM results, the material obtained by heat treatment at 80 °C is a collection of agglomerated particles with nearly spherical shape and dimensions up to 80 nm (Fig. 3). Most of the particles have a size about 40 nm.

The surface layer of particles with the thickness of 8–10 nm is characterized by crystalline order, and the interior hollow spaces within the particles are partially filled with amorphous material. The shell of spherical particles is composed of 7–9 S–Mo–S layers (Fig. 2a). According to Ref. [6], the number of layers is controlled by the CTAB concentration in the hydrothermal solution. The energy dispersive X-ray spectroscopy gave the information about the relative contents of molybdenum and sulfur atoms in the sample that are 15.8 ± 0.6 and 27.0 ± 0.6 at.% (the ratio S/Mo is 1.71), respectively. In our case, the distance between the layers ranges from 0.85 to 1.05 nm. Analyzing the data from EDS line profile (Fig. 3c), the periodicity of maxima and minima of intensity are observed (Fig. 4). Statistical calculations of these results showed that maxima of intensity repeat with the period of 0.88 ± 0.02 nm, and minima with 0.85 ± 0.02 nm, and proved the formation of periodic layered structure. Regarding the bulk samples of MoS_2 this distance is about 0.62 nm and the increase of interlayer distance can be explained by the carbon layer existence, which is confirmed by several authors [6, 18, 8]. Summing XRD, TEM, and EDS experimental data we can affirm the formation of the double-hierarchical structure MoS_2/C. The amount of carbon in the material is about 46.8 ± 0.4 at.%, with small presence of oxygen.

Annealing at 500 °C causes destruction of the spherical particles and disorientation of the layers formed from blocks of S–Mo–S (Fig. 5). There is a significant number of ragged layers, the distance between them varies irregularly. The relative contents of molybdenum and sulfur atoms in the sample are 13.0 ± 0.6 and 23.0 ± 0.5 at.% (the ratio of S/Mo is 1.77), respectively. After annealing, carbon and oxygen contents did not significantly changed (53.9 ± 0.5 and 10.1 ± 0.2 at.%, respectively). The annealing has little effect on the ratio between the contents of sulfur and molybdenum atoms, indicating the temperature stability of the structure. At the same time the question about the existence and content of carbon in the material arises.

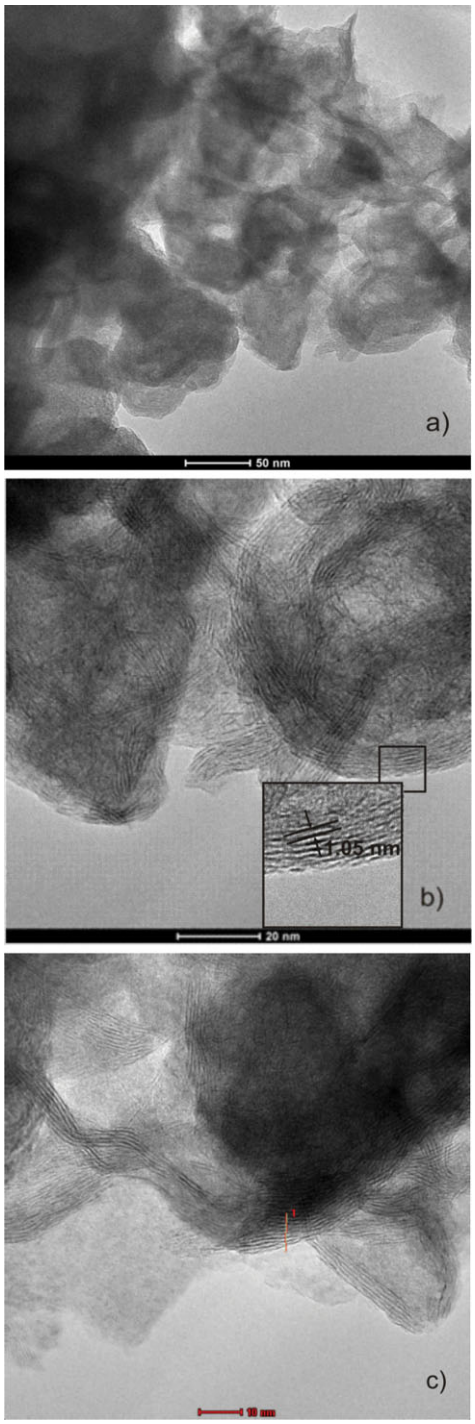

Figure 3 TEM images of the material obtained by hydrothermal synthesis after heat treatment at 80 °C (image (c) is EDS line profile).

4 Discussion The process of material synthesis can be described by the next model. Hydrothermal treatment

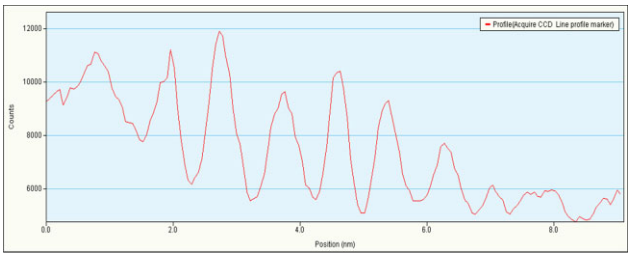

Figure 4 EDS line profile.

involves the following reactions in an autoclave (Eqs. (2) and (3)):

$$2(NH_4)_2MoS_4 + N_2H_4 \rightarrow 2MoS_2 + 4H_2S + 4NH_3 + N_2, \quad (2)$$

$$MoS_4^{2-} + N_2H_4 \rightarrow 2MoS_2 + N_2 + S^{2-} + H_2S. \quad (3)$$

In aqueous solution of $C_{19}H_{42}BrN$, there is the formation of spherical and lamellar micelles, and the dominance of second ones occurs when the surfactant excess concentration is over the value of 0.05 gcm^{-3} [19, 20]. Under the applied experimental conditions in the reaction medium both types of micelles were present. The hydrodynamic diameter of the spherical micelles, according to Ref. [21], is about 5.3 nm at the micelle concentration of 4×10^{-4} gcm^{-3} (1.5 cmc); micelle is formed of 91 monomers of the cetyltrimethylammonium bromide (CTAB). The average size of lamellar micelles is about 44 nm; however, authors of Ref. [22], recorded significant flexibility of micelles, and observed a formation of the rings with diameters of 4.5–6 nm. Thus, in the sol the micelles of both types were formed (Fig. 6b).

The electrostatic interaction between the $[MoS_4]^{2-}$ complexes and positively charged parts of surfactant molecules is the driving force of adsorption on the micelle surface (Fig. 6c). The most probable formation mechanism for multilayer structure units is shown in Fig. 6d. The creation of such ion–pair complex not only determines the particular shape and size of synthesized particles but also the surfactant serves as a catalyst due to simply increasing of the reactants concentration at the water/micelles interfaces [24, 26]. The products of dissociation of surfactant ions encapsulated in the interlayer space are fixed as the carbon-containing layer between individual sheets of 2H-MoS_2 (Fig. 6e). Annealing at 500 °C causes partial destruction of the spherical particles and disorientation of the layers due to gas release during the final decomposition of organic component. The model is consistent with the results of direct observations of the growth of the interlayer distance. Similar results were obtained by the authors of Ref. [18].

The potential use of the synthesized material in catalysis and electrochemistry depends on its morphological characteristics. The value of the specific surface area S_{sp} of the material calculated by BET method is about 15 $m^2 g^{-1}$ and increases after annealing at the temperature of 500 °C up to 32 $m^2 g^{-1}$.

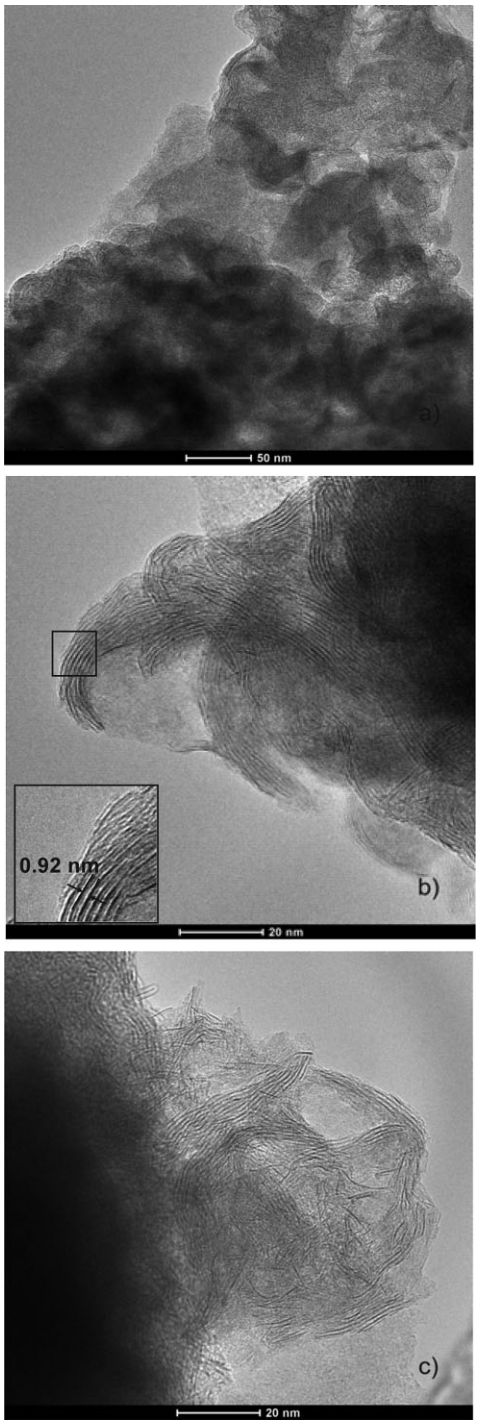

Figure 5 TEM images of the material obtained by hydrothermal synthesis after heat treatment at 500 °C.

Figure 7 shows the nitrogen sorption isotherm for synthesized material after annealing at 500 °C in Ar atmosphere. The isotherm is H3 type and has a hysteresis loop, that can be associated with sorption process inside micropores, capillary condensation within mesopores, and adsorption on external surface of the nanoparticles [25]. Analysis of this isotherm

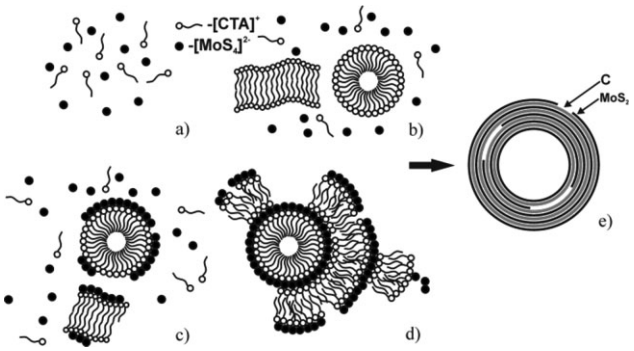

Figure 6 The proposed mechanism of nested nanospheres of 2H-MoS_2.

allowed to obtain pore size distribution and pore parameters of the annealed material (Fig. 8).

More information on morphological features of the obtained materials was received from small-angle X-ray scattering (Figs. 9a and 10a). For data analyzing, we used the procedure mentioned in Ref. [23]. Curves obtained for the material (Fig. 9a), can be divided into three angular regions with good dependence of the scattering intensity on the module of the wave vector $I(s)$ ($s = \frac{4\pi}{\lambda}\sin(\theta)$, 2θ is the scattering angle). In the (s_{min}, s_1) range, the scattered intensity is described by Guinier's law (Eq. (4)) and corresponds to the scattering of X-ray by MoS_2 nanoparticles (where R_g is radius of inertia of the nanoparticles).

$$I(s) \sim \exp\left(-\frac{1}{3}R_g^2 S^2\right). \quad (4)$$

In the (s_1, s_2) range, the intensity decline is observed, with $n \approx 4.8$. This result indicates the diffuse scattering by blurred surface, for which the change in density is typical. The (s_2, s_{max}) range probably corresponds to the scattering

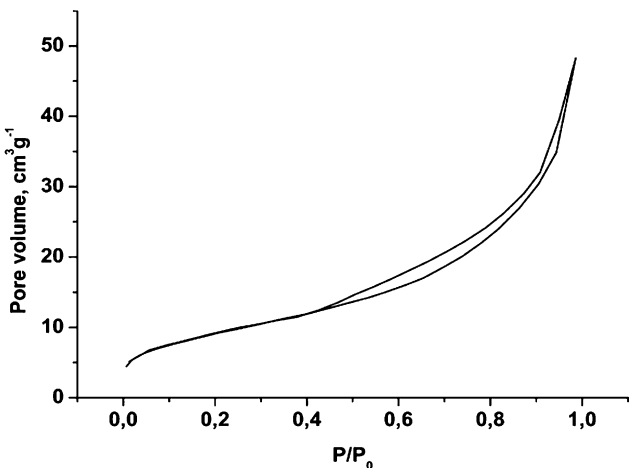

Figure 7 Nitrogen sorption isotherm for synthesized material after annealing at 500 °C.

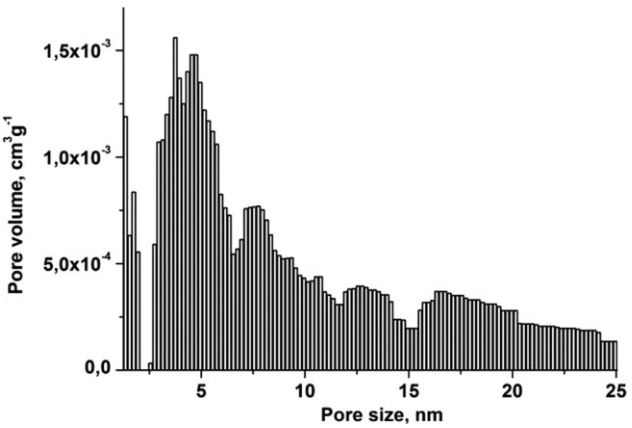

Figure 8 Pore size distribution for synthesized material after annealing at 500 °C.

by polydispersed system of mesopores. Restored distribution function of scattering centers (Fig. 9b) is characterized by a broad symmetrical peak at $d \approx 52$ nm, corresponding to the most probable diameter of MoS_2 nanospheres. The volumetric distribution function was calculated using the model of polydisperse homogeneous spheres.

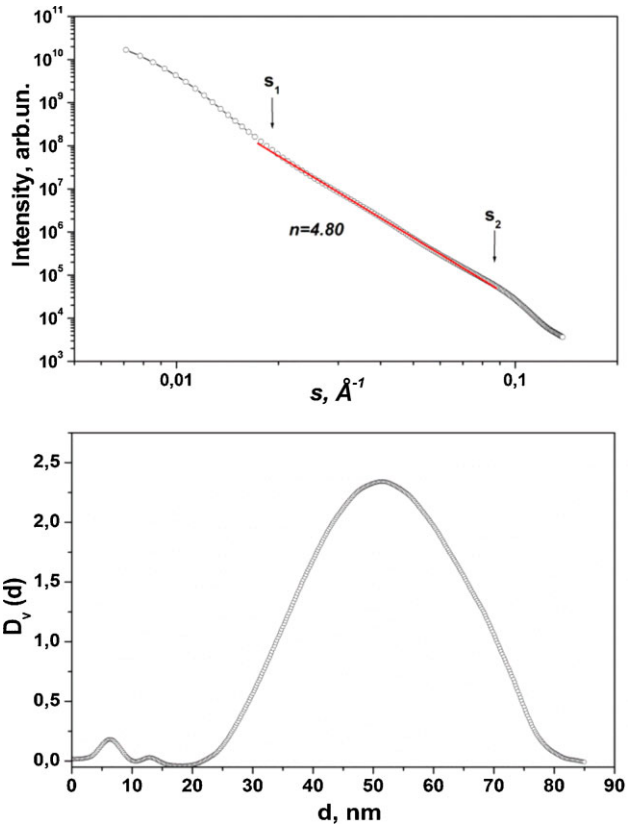

Figure 9 The curves of scattering intensity of X-rays at small angles (a) and calculated scattering centers distribution function (b) for the samples annealed at 80 °C.

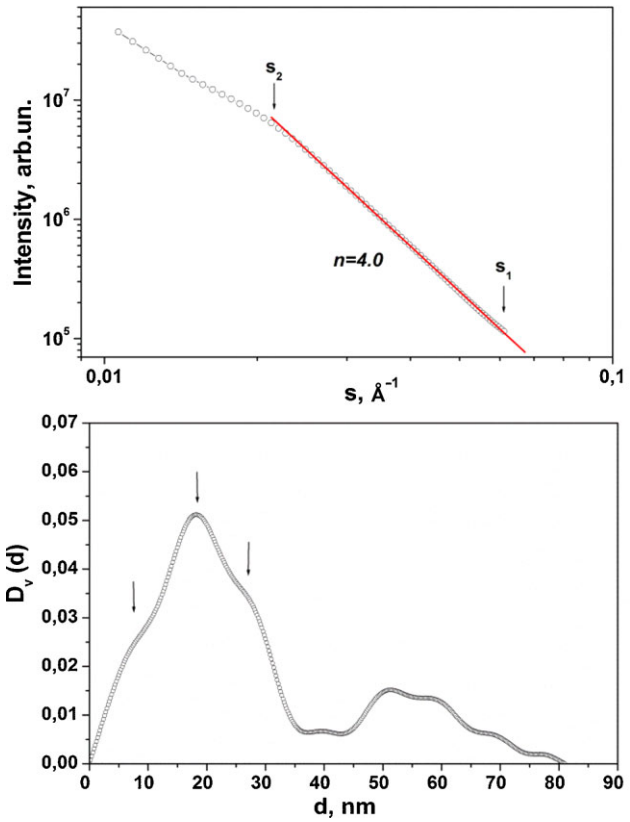

Figure 10 The curves of scattering intensity of X-rays at small angles (a) and calculated scattering centers distribution function (b) for the samples annealed at 500 °C in argon atmosphere.

For the material obtained by annealing at 500 °C, there are significant changes in the distribution of inhomogenities (Fig. 10a). It should be noticed that the significant decrease in the scattering intensity, especially in the range of 0.1–1.0 angles, is due to the decrease in the relative content of inhomogenities with the size over 40 nm. In the (s_1, s_2) range, the intensity decline is observed with $n \approx 4.0$, indicating the implementation of the Porod's law of scattering by smooth (nonfractal) surface. This behavior indicates the presence of some scattering by graphene-like surfaces.

Also there is the substantial increase in the proportion of mesopores. On the distribution function of scattering centers for this sample (Fig. 10b), there is a main peak at $d = 18.4$ nm and additional two at 7.6 and 27.1 nm, which likely reflect the probable mesopore diameters. At the same time, there is the presence of centers with characteristic dimensions in the range of 45–70 nm.

5 Conclusions Multilayer nanoparticles with the size of 40–70 nm are synthesized by hydrothermal synthesis using cations of the cetyltrimethylammonium bromide as micelle-forming agent. The resulting material has a double-hierarchical structure in which MoS_2 layers alternate with carbon. It has reported about the growth of the interatomic distances of obtained nanostructured MoS_2 within the (001) crystallographic plane and shown the formation mechanism of multi-layered nanospheres. The annealing at 500 °C leads to the destruction of MoS_2 nanospheres and the formation of mesopores with the sizes in the vicinity of 18 nm. The atomic ratio between Mo atoms and S atoms did not change, indicating the temperature stability of the structure.

References

[1] I. Wiesel, H. Arbel, A. Albu-Yaron, R. Popovitz-Biro, J. Gordon, D. Feuermann, and R. Tenne, J. Nano Res. **2**, 416 (2009).
[2] J. Tannous, F. Dassenoy, I. Lahouij, T. Le Mogne, B. Vacher, A. Bruhács, and W. Tremel, Tribol. Lett. **41**, 55 (2011).
[3] X. H. Hou, C. X. Shan, and K. L. Choy, J. Surf. Coat Technol. **202**, 2287 (2008).
[4] L. Rapoport, N. Fleischer, and R. Tenne, J. Mater. Chem. **15**, 1782 (2005).
[5] D. Chen, G. Ji, B. Ding, Y. Ma, B. Qu, W. Chen, and J. Y. Lee, Ind. Eng. Chem. Res. **53**, 17901 (2014).
[6] G. Huang, T. Chen, W. Chen, Zh., Wang, J. Ye, H. Li, D. Chen, and J. Y. Lee, Small **9**, 3693 (2013).
[7] H. Haesuk and H. Kim, and J. Cho. Nano Lett. **11**, 4826 (2011).
[8] C. Kun and W. Chen, J. Mater. Chem. **21**, 17075 (2011).
[9] A. Gupta, A. Vaishali, and V. Sukumaran, J. Phys. Chem. Lett. **6**, 739 (2015).
[10] G. Tang, J. Sun, C. Wei, K. Wu, X. Ji, S. Liu, and C. Li, Mater. Lett. **86**, 9 (2012).
[11] G. Tang, J. Sun, W. Chen, H. Tang, Y. Wang, and C. Li, Micro Nano Lett. **8**, 164 (2013).
[12] A. Varlec, S. A. Mansour, T. D. Luccio, C. Borriello, A. Bruno, J. Jelenc, and M. Remskar, Phys. Status Solidi A **210**, 2335 (2013).
[13] Zh. Wu, W. Dezhi, and S. Aokui, Mater. Lett. **63**, 2591 (2009).
[14] L. Ma, G. Huang, W. Chen, Zh., Wang, J. Ye, H. Li, D. Chen, and J. Y. Lee, J. Power Sources **264**, 262 (2014).
[15] N. Li, Y. Chai, Y. Li, Z. Tang, B. Dong, Y. Liu, and C. Liu, J. Mater. Lett. **66**, 236 (2012).
[16] Y. Zhao, X. Luo, H. Li, J. Zhang, P. T. Araujo, C. K. Gan, and Q. Xiong, Nano Lett. **13**, 1007 (2013).
[17] M. A. Lukowski, A. S. Daniel, F. Meng, A. Forticaux, L. Li, and S. Jin, J. Am. Chem. Soc **135**, 10274 (2013).
[18] K. Chang, W. Chenx, L. Ma, H. Li, H. Li, F. Huang, Z. Xu, Q. Zhang, and J. Y. Lee, J. Mater. Chem. **21**, 6251 (2011).
[19] Sh. Yan, H. Q. Luo, and N. B. Li, Spectrochim. Acta A **78**, 1403 (2011).
[20] X. Zhu, K. Hou, C. Chen, W. Zhang, H. Sun, G. Zhang, and Z. Gao, High Perform. Polym. **27**, 207 (2015).
[21] B. Naskar, A. Dan, S. Ghosh, V. K. Aswal, and S. P. Moulik, J. Mol Liq **170**, 1 (2012).
[22] Z. Lin, J. J. Cai, L. E. Scriven, and H. T. Davis, J. Phys. Chem. **98**, 5984 (1994).
[23] P. V. Konarev, V. V. Volkov, A. V. Sokolova, M. H. Koch, and D. I. Svergun, J. Appl. Crystallogr. **36**, 1277 (2003).
[24] J. Fendler, Catalysis in Micellar and Macromolecular Systems (Academic Press, New York, 1975), p. 98. Republished and opened for online access by Elsevier in 2012.
[25] A. P. Karnaukhov, Adsorption. Texture of Dispersed and Porous Materials (Nauka, Novosibirsk, 1999), Vol. 217, pp. 79, 276.
[26] D. Myers, Surfactant Science and Technology (John Wiley & Sons, Hoboken, 2006), Vol. 206, pp. 15, 334.